Supplemental Material on Liquid-liquid phase transitions in silicon.

M.W.C. Dharma-wardana* and Dennis D. Klug†
National Research Council of Canada, Ottawa, Canada, K1A 0R6

Richard C. Remsing
Rutgers University, Department of Chemistry and Chemical Biology, Piscataway, NJ 08854-8019 USA

This supplemental material provides details on the following. (1) Extending supercooled l-Si studies to equilibrium l-silicon at higher T. (2) The nature of the liquid-liquid phase transitions. (3) Details of DFT-MD calculations. (4) Theory: (a) The neutral-pseudo-atom (NPA) method : (b) Details of Kohn-Sham bound-states of the Si-ion in l-silicon. (c) Pseudopotentials, pair potentials, PDFs, and the electrical conductivity. (d) calculations in the NPA. (5) Results: (a) Robustness of the discontinuities in the Free energy. (b) The compressibility and the static conductivity. (c) LPTs as a cooperative transfer of ions from the 1st shell, as revealed by the pair potentials and PDFs of LDL and HDL silicon. (d) Results on the PDFs and the structure factor.

PACS numbers: 52.25.Jm,52.70.La,71.15.Mb,52.27.Gr

This supplemental material provides additional information on the following topics. The notations used in the main text will be assumed here. Readers already familiar with theoretical issues may go directly to the section on results.

1. Extending supercooled l Si studies to equilibrium l-silicon.
2. The Nature of the HDL and LDL phases.
3. Details of DFT-MD calculations
4. Theory:
   (a) The neutral-pseudo-atom (NPA) method.
   (b) Details of Kohn-Sham bound-states of the Si-ion in l-silicon.
   (c) Pseudopotentials, pair potentials, PDFs and conductivity.
   (d) calculations in the NPA.
5. Results:
   (a) Robustness of the discontinuities in the Free energy.
   (b) The compressibility and the static conductivity.
   (c) LPTs as a cooperative transfer of ions from the 1st shell, as revealed by the pair potentials and PDFs of LDL and HDL silicon.
   (d) Results on the PDFs and the structure factor.

*Email address: chandre.dharma-wardana@nrc-cnrc.gc.ca
†Email address: dennis.klug@nrc-cnrc.gc.ca

I. EXTENDING SUPERCOOLED l-SI STUDIES TO EQUILIBRIUM l-SILICON.

While there are some experimental studies of transitions in liquid silicon as well as in polymorphic systems (some examples being references [1–3]), most investiations of the liquid-liquid phase transition (LPT) in Si are theoretical simulation studies of metastable supercooled liquid silicon with the temperature $T \sim 0.1034$ eV and near its solid density($\bar{\rho} = \sim 2.33$ g/cm^3). These studies and their interpretation have been inspired by the deep interest in the nature of liquid-liquid phase transitions (LPTs) in water with its transient tetrahedral bonding.

In this study we have extended the range of the investigations, (a) to expanded liquid silicon down to density $\bar{\rho} \sim 1.5$ g/cm^3, (b) to compressed liquid silicon with $\bar{\rho} \sim 3$ g/cm^3, (c) and to temperatures as high as 1 eV. At T higher than the melting point the LPTs are those occurring in a stable liquid.

We have identified an ionization driven transition (IDT) as well as two more liquid-liquid phase transitions, viz., LPT2 at $\bar{\rho}$ near 2 g/cm^3, and LPT3 near 3 g/cm^3, in addition to LPT2.5 which is the hitherto studied LPT near the density of 2.5 g/cm^3. Maintaining a supercooled liquid while keeping the density uniform is extremely difficult at increasing low densities due to cavitation, fragmentation and other issue. This holds for experiments, or for N atom simulations. However, the integral equation technique used by us does not allow any other solutions except the uniform liquid as long as the equations could be converged. These issues simplify at higher T, and we find that features of the LPTs exist, though greatly weakened, even at 1 eV (11,604K) in l-silicon at equilibrium.

Hence the LPTs are very robust. Consequently, the system can be conveniently studied using methods that have been developed for the study of warm dense matter (WDM). Thus their theoretical study in a wider range of densities and temperatures is justified.

Methods are available for making uniform-density

slabs of warm dense matter [4]. Ultra-fast pump-probe optical methods have already been deployed for this type of problem [5]. Given that DFT-MD-SCAN and other simulations predict an essentially nonmetallic structure for the LDL at LPT2.5, in contrast to the strongly metallic LDL predicted by the NPA-HNC, this type of difference can be detected by ultra-fast optical studies of l-Si in WDM states. The signatures of the LPTs are found in the calculated compressibility even at 1 eV, and hence refined shock-Hugoniot determinations may reveal evidence of these LPTs by their impact on the equation of state. They are of importance in materials science, geophysics, and plasma science.

II. THE NATURE OF THE LIQUID-LIQUID PHASE TRANSITIONS

The use of empirical potentials, e.g., Stillinger-Weber model (SWM) has already been fruitful in some early studies [6] where ideas from water research have been seminal to understanding l-Si. However, such model potentials have a limited range of applicability [7] and first-principles DFT provides a more reliable tool. On the other hand, in a remarkable study by Vashist *et al.* , the SWM phase diagram is worked out in detail, providing considerable insight into tetrahedral liquids. However, such models fail to take account the important features of the electron subsystem that cannot be subsumed in model potentials.

One-center DFT implemented as NPA-HNC is based on first principles. It is computationally faster than the use of phenomenological model potentials. However the strong belief, based on chemical understanding that the angular and multi-center correlations need explicit inclusion has led to the neglect of the applications of one-center DFT to complex fluids (see, however, Ref. [9]).

Morishita [10] made an early N-center first-principles study using $N = 64$, making a connection between a high-density amorphous form of Si with a strong similarity to high-density amorphous water (found only in computer simulations of supercooled water). However, no support for phase transitions was found. In a subsequent study, Morishita [11] argued that the formation of LDL-Si is driven by the growth of tetrahedral order since the coordination number N_c in the dense liquid is $\sim$6, while it is four in the solid. That N_c should tend to four on cooling is generally accepted. However, these liquids form an LDL instead of simply acquiring $N_c = 4$ by solidifying, or becoming a glass, or forming nano-crystallites, and this is a major question that needs resolution. The more fundamental reasons as to what drives the coordination number, and why an LDL may be formed instead of other alternatives, may be more clear from the pair-potentials, PDFs and the Fermi-liquid picture of $2k_F$ scattering in l-Si that we present in sec. V C.

It is not clear if a liquid state (i.e., a uniform phase) even exists between the densities intermediate to LPT2.5 and LPT2 as the calculated compressibility becomes very large and singular in this region at 1200K with negative pressure. though well behaved at higher T. The DFT-MD results are available only at the LPT2.5, where the HDL found via NPA-HNC agrees with the HDL from MD-DFT. However, the NPA-HNC finds three metallic LDLs at the three phase transitions, the DFT-MD finds a nonmetallic low density liquid (nm-LDL) at LPT2.5, whose structure factor is liquid-like at high-K, and more solid like at low-k. The nm-LDL is metastable, while the metallic LDLs of NPA-HNC are stable even at higher T. However, when T is lowered below 1200K near LPT2.5, it may rearrange to nm-LDL in a continuous manner. Hence, further studies with one-center DFT (i.e, NPA) methods as well as N-center methods applied below 1200K, and also under WDM conditions are needed to examine these possibilities.

III. DETAILS OF DFT-MD CALCULATIONS

We have used DFT-MD-SCAN simulations, as well as simulations with the PBE fuctional. However, we have used N =108 atoms in the simulation cell and adequately recover the results of Ref. [12] where many more atoms were used in the simulations, and convergence with respect to N was studied. We use an energy cut off set at 300 eV and a $2 \times 2 \times 2\,k$ grid in this work. The occupation in the highest energy state is less than 0.0001 even at the highest temperature used. The DFT-MD simulations used the SCAN functional but the Kubo-Greenwood (KG) calculations for the electrical conductivity could only use the LDA as advanced functionals are not available for KG calculations. Using pre-selected starting configurations was very helpful to generating the nm-LDL in these DFT-MD-SCAN simulations.

IV. A SUMMARY OF THE NEUTRAL PSEUDO-ATOM (NPA) METHOD.

Most of the results presented in this paper are obtained via the NPA approach which uses only uniform spherically symmetric static one-body densities for studying the liquid state. No time-dependent information, angular correlations etc., are used and a strict DFT one-body radial density-based approach is followed. MD-DFT is used to confirm or confront these results where experimental data are not available.

Here we give, for the convenience of the reader, a review of the neutral-pseudo-atom method used here, while a more detailed recent discussion based on highly compressed hydrogen may be found in Ref. [13]. We consider *a single* silicon nucleus (chosen to be the origin of coordinates), interacting with other silicon nuclei ("field ions"), and electrons. It is not necessary to assume that the Si atom is at rest. As we are dealing with a fluid, spherical symmetry is assumed, so that calculations reduce

to simple radial integrations. Unlike in standard DFT-MD simulations [14], we do not consider well-defined ion configurations in an N-ion simulation cell. Instead, the field ions are replaced by their one-body distribution $\rho(r)$ since density functional theory (DFT) posits that the free energy is a functional of just the one-body density. Thus the N-body ion problem is replaced by a one-body (i.e., one-ion) problem in the sense of DFT. This becomes exact if the ion correlation functional is exact. In practice it is approximate due to uncertainties in the XC-functionals. As only a single ion center is used in NPA calculation, we do not have a highly inhomogeneous N-center electron distribution as in standard DFT simulations [14] where several hundred ions define a very complex electron distribution in a simulation cell. Instead, just a single-center spherical electron distribution dependent on electron-electron and ion-ion correlation functionals is used. The much smoother single center electron density $n(r)$ can be conveniently treated using the local density approximation (LDA), as has been found from previous work. The electron exchange correlation functional used [15] in the LDA is a finite-T functional but we find that the finite-T effects on the electron XC-functional are completely unimportant in this problem, even at 1 eV, as expected.

The use of the single particle ion density $\rho(r)$ instead of an explicit N-center simulation leads to enormous computational economies and simplifications, but now calls for a good ion-ion XC-functional F_{xc}^{ii} in addition to the usual finite-T electron-electron XC-functional F_{xc}^{ee} used for electrons. If the Born-Oppenheimer approximation is to be avoided, we also need a form for F_{xc}^{ei}, i.e., an ion-electron correlation functional. Here we do not use an F^{ei} but follow Ref. [13] with respect to the e-e and i-i functionals. The functional derivatives of the XC-functionals with respect to the two densities provide the corresponding XC-potentials.

The electron distribution around the central nucleus is denoted by $n(r)$. Spherical symmetry is applicable for both $n(r), \rho(r)$ in the liquid state. This fact is ignored in N-center DFT simulations which treat liquids as an average over frozen periodic solids with N-atoms in the unit cell. Initially, the detailed forms of $n(r), \rho(r)$ are unknown and our objective is to determine them using the Kohn-Sham-Mermin theory at finite T for a neutral pseudoatom where the Helmholtz free energy $F[\rho, n, T]$ is a functional of *both* the one-body densities, viz., of ions and electrons. One may instead work with the grand potential $\Omega[\rho, n, T]$ where the desired particle densities are set through the electron and ion chemical potentials μ_e, μ_i. The DFT variational principles lead to *two* coupled Euler-Lagrange equations. The first of these, $\delta\Omega/\delta n(r) = 0$ leads to the finite-T Kohn-Sham equation for $n(r)$, and contains an electron-electron XC-potential, $V_{xc}^{ee}(r)$ as well as an electron-ion XC-correlation potential V_{xc}^{ei}. The latter can usually be neglected, as is the case when one makes the Born-Oppenheimer approximation.

The second Euler-Lagrange equation, from the functional derivative of Ω with respect to the ion density, viz., $\delta\Omega/\delta\rho(r) = 0$ leads to an equation for the ion density $\rho(r)$, and needs an ion-ion XC-potential V_{xc}^{ii} which usually does not need an exchange part because most ions are classical particles. It was shown in Ref. [16] that, for classical particles, a good approximation to V_{xc}^{ii} is the sum of hypernetted chain (HNC) diagrams, going beyond mean-field approximations. That is, V_{xc}^{ii} is a highly non-local quantity that is expressed in terms of the ion-ion pair-distribution function (PDF) $g(r)$. If the density of the field ions far away from the central nucleus is $\bar{\rho}$, then the ion-ion PDF is of the form $g(r) = \rho(r)/\bar{\rho}$. Furthermore, the Euler-Lagrange equation for $\rho(r)$ leads to a Boltzmann-like distribution for $\rho(r)$. Then the classical-DFT Kohn-Sham potential may be identified with the potential of mean-force well known in classical statistical mechanics of the liquid state.

The electrons will interact with the central Si nucleus and form bound states which constitute the 'bound-core' of the ion with a net charge denoted by $\bar{Z}$. These bound electrons in a silicon ion are located well within the Wigner-Seitz radius r_{ws} (see below) of silicon ions in the fluid. At the melting point, at normal pressure and density, the ion charge $\bar{Z}$ is four, consistent with the usual valence of Si. That is, there are four free electrons per ion in the metallic fluid. The electron distribution $n(r) \to \bar{n}$ (i.e., the mean electron density) for sufficiently large r. The electron Wigner-Seitz radius is:

$$r_s = r_{ws}/\bar{Z}^{1/3} = [3/\{4\pi\bar{n}\}]^{1/3} \quad (1)$$

$$r_{ws} = [3/\{4\pi\bar{\rho}\}]^{1/3} \quad (2)$$

Since the ion-ion PDF is initially unknown, we assume a very simple form of $g(r)$, denoted here by $g_{cav}(r)$, having the form of a spherical cavity for $r \le r_{ws}$, and unity for $r > r_{ws}$ and determine an initial electron density $n(r)$ from the Kohn-Sham equation, with $\rho(r) = \bar{\rho} g_{cav}(r)$. The radial Kohn-Sham equation is solved in a large sphere of radius R_c, such that all particle correlations have died down for $r > R_c$. In the present study on Silicon $R_c \simeq 13.3 r_{ws}$ and hence include the average density of nearly 10,000 silicon atoms.

For most problems, it turns out that electronic structure is insensitive to further elaborations of the $g(r)$, except for adjusting the radius of the cavity to be consistent with $\bar{Z}$ and the Friedel sum rule. This simplified form of the NPA theory is implemented in Ref. [17]. It is then computationally convenient to use the $n(r)$ obtained from the self-consistently determined "spherical cavity" PDF, viz., $g_{cav}(r)$, to construct the response of a cavity-free uniform electron gas of density $\bar{n}$ to the central ion by correcting for just the cavity response. The cavity corrected charge density pile up of free electrons, $\Delta n_f(q)$ given in k-space is then used to construct pseudopotentials, as discussed below.

The total object consisting of the central nucleus, the electronic and ionic densities $n(r), \rho(r)$ constitute a neutral object known as the neutral-pseudo-atom and occupies the whole volume of the correlation sphere.

The above approach to the many-ion, many-electron problem does not require us to make assumptions about "non-overlapping muffin tins", or make cluster expansions in the ion density or limit the method to densities such that higher clusters beyond binary pairs are deemed negligible, as proposed in many presentations of "neutral pseudo-atom" theories. For more details, the reader is referred to the relevant literature [13, 16, 18].

In effect, the NPA approach relegates the ion-ion many-body problem to the construction of appropriate ion-ion XC-potentials. Thus the NPA formulation used by us [16, 17, 19] differs in this respect from many other 'neutral-pseudo-atom' models that have been proposed, even though Ref. [17] presents the theory from the conventional approach of expanding the free energy as a function of ion density, and retaining only binary clusters. Furthermore, many 'average atom' models restrict the free-electron density to the ion Wigner-Seitz sphere by setting $R_c = r_{ws}$, as in the 'ion-sphere' models of Salpeter valid at very high temperatures [20]. Additionally, it has been shown that such models fail to define a unique mean ionization $\bar{Z}$ [21] and hence cannot satisfy the Friedel sum rule.

A. Details of the Kohn-Sham states of the Si ion in *l*-Silicon

Some details of the highest occupied Kohn-Sham states in the high-density liquid (HDL) silicon, and in the low-density liquid (LDL) silicon, obtained from NPA calculations are given in table I. This is of importance in determining if the proposed Ionization driven transition (IDT) is a physical feature or a model artifact.

The Kohn-Sham calculations show that the core electrons are compactly contained in the Wigner-Seitz sphere, and hence there is no ambiguity in defining a mean ionization by $\bar{Z} = Z_N - n_b$, where $Z_N = 14$ is the silicon nuclear charge, while n_b is the total number of electrons in the bound core. That is, we are not dealing with resonances in the continuum which make it difficult to define free and bound electrons clearly. The value of $\bar{Z}$ is also subject to a very strong consistency test as the phase shifts of the continuum states must satisfy the finite-T Friedel sum rule [16]. This is satisfied to better than $\sim 98\%$ in our calculations.

If the bound states while ionizing into the continuum becomes resonances the definition of $\bar{Z}$ becomes problematic. Furthermore even if no such problems with resonances occur, the continuum states are modified as they acquire phase shifts. Average-atom calculations which ignore such modifications of the continuum show unphysical discontinuities in physical properties when ionization is described by such models [22]. In our NPA model the changes in the continuum density of states (DOS) and effects of phase shifts are taken into account, and hence the current NPA model does not suffer from this problem.

The limitations of the electron XC-functional are relevant, just as in N-center DFT, although perhaps not to the same extent. The energy gap associated with the movement of a bound state from the atomic core to the continuum is inadequately described by DFT, just as the band-gaps in solids are incorrectly given by standard DFT, as the objective of DFT is the total energy and not individual electron states. Hence, the prediction of the IDT suffers also from our lack of knowledge of the discontinuity that is said to be present in the electron XC-functional [23]. This problem exists with N-center DFT algorithms (e.g, the VASP code) or with one-center methods like the NPA based DFT theory. As a consequence, the density of states (DOS) as well as bandgaps determined using DFT (or NPA) are those of the fictitious non-interacting electrons of Kohn-Sham theory, and they need not agree with experiment. As such, when accurate band gaps or DOS are required, one is obliged to resort to approximate solutions of the Dyson equation (as in the GW approach), or use XC-functionals that are designed for getting good bandgaps, while failing with respect to some other properties. Correct calculations of the valence band gap is needed for the prediction of metallic states versus insulators, as is the case with the LDL in *l*-Si.

TABLE I: Kohn-Sham energies ϵ_{nl} (a.u.) and occupations f_{nl} for HDL and LDL Si at the densities ρ in g/cm^3. Here the Fermi factors $2f_{nl}$ includes spin. The bound-states with radii $< r >$ in a.u., are well inside the Wigner-Seitz sphere with $r_{ws} = 3.08$ a.u. for HDL and 3.21 a.u. for LDL Si at $\bar{Z} = 4$. Thus the definition of $\bar{Z}$ involves no ambiguity. The case 1.5 g/cm^3 is the $\bar{Z} = 3$ state, $r_{ws} = 3.7146$ which is possibly the progenitor of LDL-Si as studied by, e.g., Remsing *et al.* [12]

density ρ	state	$-\epsilon_{nl}$	$2f_{nl}$	$< r >$	$Z = 14 - n_b$
2.574	$2s$	8.769	2.0	0.573	
	$2p$	5.648	2.0	0.540	4.0
	$3s$	-	-	-	
2.270	$2s$	8.851	2.0	0.573	
	$2p$	5.730	2.0	0.540	4.0
	$3s$	-	-	-	
1.500	$2s$	9.919	2.0	0.573	
	$2p$	6.078	2.0	0.539	
	$3s$	1.013	1.0	0.547	3.0

B. Construction of the pseudopotential

The free-electron density pileup $\Delta n(r) = n(r) - \bar{n}$ around a single silicon ion placed in the medium with a spherical cavity around the nucleus is used, after a cavity correction, to construct a pseudopotential $U_{ei}(r)$. The pseudopotential is then used to construct a Si-Si pair-potential $V_{ii}(r)$. It turns out that for metallic fluids, it is usually possible to define a linear-response local pseudopotential $U_{ie}(r)$ that includes the non-linear

effects of the Kohn-Sham calculation by construction. The pseudopotential in k-space is defined first and the r-space form may be obtained via a Fourier transform. The bound state density $n_b(r)$ is fully contained in the Wigner-Seitz sphere of the ion, while the total electron density $n(r)$ extents to the edge of the correlation sphere $R_c \sim 10r_{ws}$. So we define

$$\begin{aligned} n_b(r) &= \Sigma_j 2(2l+1) f(\epsilon_j, T)|\phi_j(r)|^2,\ j = n, l \quad (3) \\ f(\epsilon_j, T) &= [1 + \exp\{(\epsilon_j - \mu^0)/T\}]^{-1} \quad (4) \\ \Delta n(r) &= n_f(r) - \bar{n},\ \ n_f(r) = n(r) - n_b(r) \quad (5) \\ U_{ei}(q) &= \Delta n(q)/\chi(q, T) \quad (6) \end{aligned}$$

The solution of the Kohn-Sham equation within the correlation sphere yields the eigenvalues and eigenfunctions $\epsilon_j, \phi_j(r)$ for the fictitious Kohn-Sham electrons whose only purpose is to give the correct one-body density. For bound states, the index $j = n, l$ applies, where n, l are principle and azimuthal quantum numbers respectively, with the spin and magnetic quantum numbers summed over. The fully interacting finite-T electron-electron response function $\chi(q, T)$ used in Eq. 6 can be expressed in terms of the Lindhard function, local field corrections $G_q(T)$ inclusive of an effective mass for electrons as discussed in [24] and other work. Here $\Delta n(q)$, the Fourier transform of the free electron part of the *nonlinear* charge density pileup $\Delta n(r)$ obtained from the Kohn-Sham equation is used to construct a *linear response* pseudopotential. The limits of validity of such procedures are discussed in [24]. If the density pileup $\Delta n(q)$ were resolved into angular momentum components, then non-local pseudopotentials can be defined. However, in this work we have found that a local (i.e., s-wave) linear-response pseudopotential is quite sufficient. In the case of the HDL, we get good agreement with available DFT-MD results for the PDFs, $S(k)$ and the static conductivity evaluated by entirely different methods. However, the DFT-MD-SCAN predicts a very different nonconducting structure which is solid-like in its $S(k)$ for small-k (i.e., large r), and liquid-like near $k_F - 2k_F$ (small r). The NPA procedure predicts a Low density liquid produced by strong $2k_F$ scattering but still remaining a good conductor, even at 1 eV. The corresponding calculations with DFT-MD-SCAN at 1 eV are not currently available. In this context we note that the LPT2.5 is predicted to occur in the same density region by the NPA-HNC and by DFT-MD.

C. The pair potential

Once the pseudopotential $U_{ei}(q)$ is available, the pair-potential can be written down without solving a 2-body Schrödinger equation since $U_{ei}(q)$ is linear in the electron response by construction. Hence the pair potential $V_{ii}(q)$ can be written down in second-order perturbation theory as:

$$V_{ii}(a) = \bar{Z}^2 V_q + |U_{ei}|^2 \chi(q),\ V_q = 4\pi/q^2. \quad (7)$$

For convenience, the pseudopotential may be fitted to some analytic form such as the Heine-Abarankov form where the effective "core-radius r_c associated with the potential may be explicitly introduced. Thus

$$U_{ei}(r) = A, r < r_c,\ U_{ei} = -\bar{Z}/r,\ r > r_c. \quad (8)$$

Usually, the fit is done in q-space and values of $q > 2k_F$, where k_F become rapidly unimportant (for $T < E_F$) and need not be fitted. However, in this work we do not use a fitted form but directly use the pseudopotential from Eq. 8.

D. The NPA-HNC calculation of the PDFs of liquid Si.

Unlike in DFT-MD where the silicon liquid is treated as a periodic crystal with a unit cell of N atoms, with $N \sim 108$, or 216 etc., the NPA treats l-Si as a highly degenerate electron liquid (Fermi liquid) containing scattering centers. Such a picture is feasible as long as there are conducting electrons in the system. Since the bonding is transient, for sufficiently long time scales ($\omega \to 0$) all "transient-bonding" electrons delocalize to give a uniform free-electron density consistent with the $\bar{Z}$ calculated from the NPA. In the Fermi-liquid picture the electron localization implies an effective mass m^* dictated by the average local transient band structure of the liquid contributing to the self energy of the one-body electron propagator.

In Ref. [25] an effective electron density parameter r_s^* was introduced into the electron response function $\chi(k)$ as follows.

$$\begin{aligned} V_k\chi(k) &= V_k\chi^0(k)/\left[1 - V_k(1 - G_{k,\lambda})\chi^0(k)\right] \quad (9) \\ &= 4\lambda^* F^0(k)/\left[k^2 - 4\lambda^*(1 - (G_{k,\lambda^*})F^0(k)\right] \\ V_k &= 4\pi/k^2,\ \lambda^* = \alpha r_s^*/\pi,\ \alpha = (4/9\pi)^{1/3} \quad (10) \end{aligned}$$

Here the dimensionless Lindhard function $F^0(k)$, with k in units of the Fermi wavevector has been introduced. As noted by March [26], this is equivalent to the use of an effective electron mass m^* differing from unity, or to an effective electron density different from the nominal value, at the Fermi energy E_F, due to electron renormalization effects. An electron effective mass of ~ 1.1 has been used in these NPA calculations for liquid Si, as in Ref [24].

Modifications in the density of states $D(E), m^*$ at the Fermi energy translate into modifications in electron scattering (at $q = 2k_F$) and lead to a special feature in $S(k)$ arising from the competition of two length scales, viz., the ionic Wigner-Seitz radius r_{ws} which defines packing effects, and the inverse Fermi wavevector which defines electron scattering and localization effects which ultimately lead to covalent-bonding effects.

The usual computer snap shots of transient covalent bonding found in DFT-MD simulations of liquid C, Si

etc., are well known [27]. Recent simulation studies have shown that these transient covalent bonds have a life time of the order of 0.6 ps [28]. Only the spherical average of correlations survives after sufficiently long times scales implied by $\omega \to 0$. The resulting static correlations are captured in the time-independent PDFs calculated by the NPA approach, and from DFT-MD simulations of $g(r)$. Furthermore, the PDFs obtained from the NPA approach, based on a single ion-center and an ion correlation functional based on hypernetted chain diagrams are in good agreement with the PDFs obtained from the multi-ion simulations (e.g., $N \sim 108$) of DFT-MD, as has been explicitly checked for many cases like Al, Li, C, Si, Be, H, etc [29–32].

Unlike in DFT-MD where the small-k limit of the structure factors $S(k)$ cannot be accessed since the simulation is done in a box of linear dimension L, the NPA uses a very large correlation sphere of radius $R_c \simeq 13 r_{ws}$ and very small values of k are accessible. We discuss our results for the PDFs and structure factors in the following section. The so obtained $S(0) = \kappa_T/\kappa_T^0$ is presented in panel (b) of 2.

The Fermi liquid picture of C, Si, Ge used within the NPA model was discussed already in the 1980s in Ref. [9] where the results from Car-Parrinello simulations were compared with NPA-type calculations. They provided a complementary picture to the chemical picture of transient covalent bonds in terms of strong scattering near $k = 2k_F$, where k_F is the Fermi momentum, as discussed below.

E. Conductivity

Although the NPA model provides a full set of KS eigenstates, we do not use the Kubo-Greenwood (KG) formula [33] to calculate the dynamic conductivity as our primary objective is the static conductivity σ. Density functional theory as used in the NPA is a static theory with no information on actual electron eigenvalues or bandgaps. Instead we use the Ziman formula as it uses only static quantities, and directly provides the static conductivity. It avoids the need to use a Drude fit or some such model to take the static-limit of the dynamic conductivity given by the KG formula. However, in getting the static conductivity both the KG and the Ziman formulae use the additional ansatz of a momentum-relaxation time τ_{mo}. It was shown in Ref. [34] that the Ziman formula within the NPA gives good agreement with experiment (where available) for the metallic liquids and plasmas studied there.

The Ziman formula has been successfully used for decades for predicting conductivities of liquid metals and their mixtures [35]. It calculates the inverse of the conductivity, i.e., the resistivity, via a force-force correlation function rather than via the Boltzmann equation. It is believed that this sums a different class of diagrams giving better agreement with experimental conductivities. One of the "issues" that arises in conductivity calculations using the Ziman formula is the question of how to include the modifications to the conductivity arising from the electron effective mass m^*. Various views have been expressed on this (see, e.g., [36]). The Drude formula $\sigma = \bar{n}e^2\tau/m^*$, where τ is the mean momentum randomization time, involves an effective mass m^*. Similarly, the electron-response function involves the electron effective mass. We include the effect of m^* only in the screening function, according to the description given in Eq. 10.

Even at the highest temperature studied here (1 eV) in the context of the LPT, the electrons in l-Si are strongly degenerate as $T/E_F \sim 0.077$ and hence the behaviour of m^* near the Fermi energy is critical. Unlike in simple metals, we see from Fig. 6 that renormalization effects near the Fermi energy are very important for the Fermi liquid description of liquid Si. The chemical picture emphasizes the formation of transient covalent bonding using valence electrons. These are the electrons near the Fermi energy and the chemical picture is consistent with the Fermi-liquid picture.

The DFT-MD-KG approach involves using the static ionic positions obtained from a DFT-MD equilibration to calculate the Kubo-Greenwood dynamic conductivity for a sufficiently large number of ionic structures further evolved and re-equilibriated from the initial ionic configuration. However, the KG algorithms available with the more common packages implement only the LDA, and do not have the SCAN and other advanced functionals that may have been used to generate the PDFs. That is, although the initial equilibriation is done with the SCAN functional, the conductivity $\sigma(\omega)$ is calculated within LDA. Furthermore, volume fluctuations are associated with density fluctuations in the simulation process, and the nominal density is obtained only as an average. Although KG requires the use of true single-particle eigenstates (SPE) and energies (e.g., by a solution of the Dyson equation), the Kohn-Sham states and Kohn-Sham energies are used in KG in lieu of the true SPE.

Further more, unexpectedly large numbers of particles ($\sim$ 1500) and large k-grids have been found necessary to get accurate results in simulations of even some simple metals like sodium [37]. Migdal et al [38] have also studied the behaviour of Kubo-Greenwood calculations for Si as a function of XC-functionals, grids, as well as the number of particles in the simulation. They too find that their PDFs do not agree with experimental data much beyond the first peak.

In spite of these difficulties, calculations of $\sigma(\omega)$ and the $\omega \to 0$ limits have been carried out successfully, especially in cases where the extrapolation to $\omega \to 0$ could be done by a fit to the Drude form of $\sigma(\omega)$. As seen from Fig. 6 of the main text, the assumption of a Drude form for $\sigma(\omega)$ is problematic for liquid Si near the LPT. In view of these difficulties, we have used a "grosso-modo" estimate of the $\omega \to 0$ limit of $\sigma(\omega)$ and displayed the data in Fig. 7 of the main text, and LDL-HDL data in Fig. 2. DFT-MD and NPA results for the conductivity

of the HDL agree. These estimates of the conductivity are only in qualitative agreement with experimental data, available at present only for the HDL. However, the calculations show a sharp decrease in the static conductivity at the HDL→LDL transition from the DFT-MD simulation, more than expected from the change in density. The sharp change in the *character* of $\sigma(\omega)$, showing a sharp drop in the static conductivity, while showing a high conductivity corresponding to what may be interpreted as a mobility edge is of great interest (see Fig. 6 of the main text).

V. RESULTS

A. Robustness of the discontinuities in the Free Energy.

So far the l-Si LPT has been studied only in a supercooled liquid, i.e., under metastable conditions. We find that there are robust LPTs for liquid Si under equilibrium even at 1 eV. Here we briefly outline the calculation of the free energy, and present relevant results.

The NPA equations generate pseudopotentials, pair potentials, and pair-distribution functions using only the Kohn-Sham densities for the given conditions of the fluid, as discussed below. The total free energy is easily calculated from the results, as discussed in Refs. [17, 19]. The total free energy per atom for a given ionic configuration (expressed as the density distribution $\rho(r) = \bar{\rho}g(r)$ around a given Si nucleus) can be expressed as:

$$F_e = F_{id} + F_0 + F_{em} + F_{12} - E^0_{at} \qquad (11)$$

The energy of an isolated atom at $T = 0$ in its ground state, E^0_{at}, is used as the reference energy. Here F_{id} is the classical ideal-gas energy of the non-interacting ion subsystem per atom. Each atom contributes $\bar{Z}$ free electrons to the electron fluid. F_0 is the free energy of $\bar{Z}$ electrons in a uniform electron gas, with a kinetic energy component and an XC-component. F_{em} is the "embedding free energy" of a neutral pseudo atom. This is defined as the difference between the free energy of the electron gas of mean density $\bar{n}$ with and without the NPA. The F_{12} term contains the free energy contributed through the ion-ion pair-distribution function and the pair-potential. Hence this is effectively the XC-free energy of the classical ions, or in more conventional language, the 'bonding energy' of two ions immersed in the fluid with average densities $\bar{n}, \bar{\rho}$. If the two ions carry further bonding their effects are also included automatically via their signatures in the PDFs.

In the HNC approximation, the main contribution to F_{12} is an integral of the pair-potential weighted by $h(r) = g(r) - 1$, whereas, more generally it involves a coupling constant integration. As bridge contributions evaluated via Lado-Foils-Ashcroft criterion were found to be negligible, the HNC approximation holds and no coupling-constant integration was used. So the calculations could follow the method outlined in Ref. [17]. Detailed expressions and methods for calculating the above quantities may be found in Refs. [19] or e.g., in Eq. 25 of of Ref. [17] and its Appendices A and B.

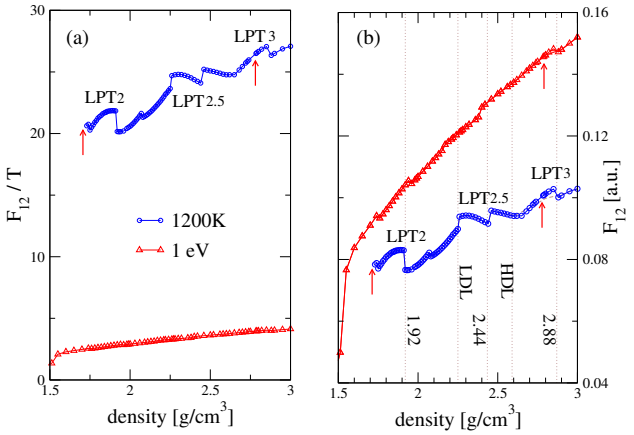

FIG. 1: (Online color) The bonding (structural) contribution to the Free energy, viz., F_{12} is shown as a function of the density for two temperatures. Panel (a) shows F_{12}/T where we see that the discontinuities in the free energy become less significant at higher T due to scaling with T, as compared to the case of T=1.0 eV. However, Panel (b), where the absolute' value of F_{12} is given in Hartree atomic units, shows that the discontinuities persist even at 1 eV. It is not a property specific to the supercooled metastable liquid, or a result of numerical artifacts of low -T calculations. The dotted vertical lines show that the positions of the discontinuities and the LPTs in the supercooled l-Si are nearly similarly located at higher T.

We display F_{12} versus the density at constant T in Fig. 1 and demonstrate that the discontinuities are robust even up to 1 eV. The NPA-HNC failed to converge between $\bar{\rho} = 2.74$ g/cm^3 and 2.78 g/cm^3, prior to the onset of LPT3, and this feature held for intermediate temperatures between T =0.1034 eV (1200K) and even at 1 eV (the highest temperature studied). Only the data at 1 eV and 0.1034 eV are reported here. The convergence was also very hard for $\rho < 1.74$ g/cm^3 at 1200K. No DFT-MD studies at the IDT, LPT2 or LPT3 are available. Nevertheless, these results show that the LPTs are not transient features of a metastable supercooled liquid, but become stable features when the temperature is above the melting point, and for $T < E_F$ when electrons are partially degenerate and capable of transient bonding. When $T \leq E_F$ the scattering of electrons is dominated by $2k_F$ processes and leads to a splitting of the $S(K)$ near $2k_F$, creating new ionic structures in the fluid.

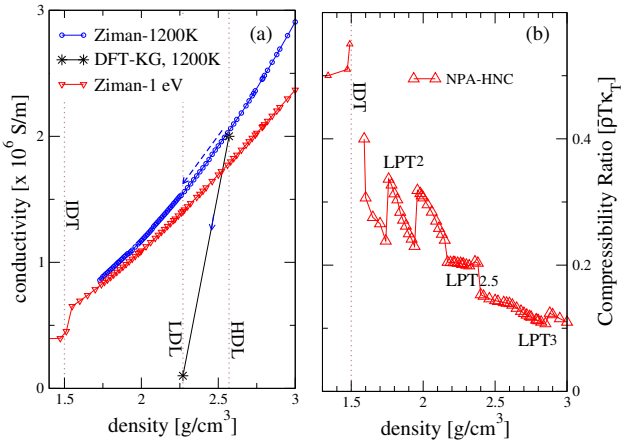

FIG. 2: (Online color)(a) The static conductivity σ as a function Of $\bar{\rho}$ for two temperatures. The DFT-MD-SCAN result for σ of the LDL at LPT2.5 is found to be virtually non-conducting, giving a large change in σ from the HDL and the LDL (arrow). The NPA-HNC-Ziman calculation finds a metallic LDL with a more modest decrease in σ from the HDL (dashed arrow). The increase in T leads to a modest decrease in σ as for a poor metal, especially at low T. Panel (b) shows that the compressibility even at 1 eV contains strong signatures of the IDT, LPT2, LPT2.5 and the LPT3.

B. The compressibility and the static conductivity

The compressibility, the electrical conductivity $\sigma(\omega)$ and its static limit σ are properties that may be used for the experimental detection of the phase transitions in a fluid at the proposed temperatures. The isothermal compressibility κ_T can be studied using shock-wave techniques and acoustic measurements.

The dynamic conductivity $\sigma(\omega)$ and its static limit are available from X-ray Thomson scattering, as well as ultrafast laser pump-probe methods. Optical conductivity can distinguish been a metallic phase and a non-metallic phase. Hence we present, in Fig. 2, panel (a) the static conductivity. Some theoretical aspects of conductivity calculations are taken up below in sec. IV E.

We display in panel (b) the isothermal compressibility ratio κ_T/κ_T^0, where κ_T^0 is the ideal gas compressibility $\bar{\rho}T$. This ratio is determined from the small-k limit of $S(k)$ as an independent property directly linked to the structure of the fluid, rather than from a pressure calculation starting from the free energy that we already know has discontinuities.

Since the HNC approximation does not accurately satisfy the compressibility sumrule, especially at low T, we present the $T = 1$ eV κ_T data in panel (b). The $S(k)$ calculations at higher T run smoothly and do not face hysteresis-like effects and convergence difficulties found at 1200K.

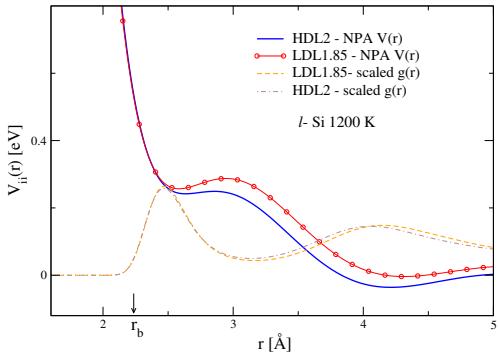

FIG. 3: (Online color) The NPA generated pair potentials for the HDL and the LDL at the LPT2 for expanded l-Si near 2g/cm^3 are displayed, together with the corresponding $g(r)$. The minimum in the Friedel oscillation is further out, and accommodates the reduced density as compared to the HDL.

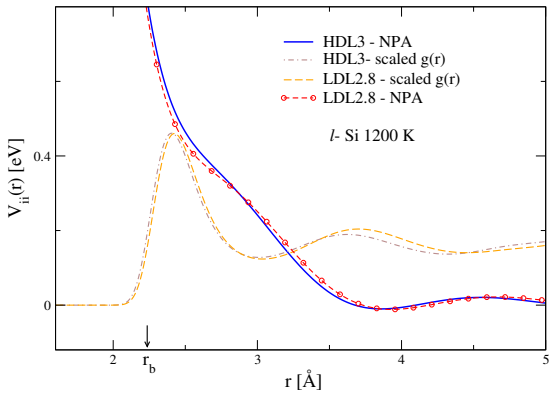

FIG. 4: (Online color) The NPA generated pair potentials for the HDL and the LDL at LPT3 in compressed l-Si near 3g/cm^3 are displayed, together with the corresponding $g(r)$. The minimum in the Friedel oscillation is further out, and accommodates the reduced density as compared to the HDL.

C. LPTS as a cooperative transfer of ions from the 1st shell, as revealed by the pair potentials and PDFs of LDL and HDL silicon.

We examine the pair-potentials and the PDFs at the LPTs to understand the origin of the LPTs. The data suggest that the LPTs occur due to cooperative transfer of an ion from the 1st coordination shell to the next, which is at a minimum of a Friedel-oscillation, The length scale of the Friedel oscillations are set by the inverse of the Fermi wave vector k_F.

Pair potentials obtained from the NPA for silicon ions in the HDL, and in the LDL at 1200K for the expanded liquid are shown in Fig. 3. Figure 4 presents similar data for the compressed liquid. Although the density has decreased in the LDL, the first-peak of the HDL falls on

the 1st peak of the LDL, showing that the coordination number N_c in the first shell has decreased. This is seen to hold for all three LPTs, with the plots for the LPT2.5 given in the main text. With $N_c = 6$ in the first shell at LPT2.5 [11], the densities 2 g/cm^3 and 3 g/cm^3 at the LPT2 and LPT3 correspond to $N_c = 5$ and 7 respectively. Hence, at each transition, an ion is transferred out of the 1st shell.

Although our estimates of coordination numbers may be in error by about one, a change of N_c by unity at each LPT is more firm. Given that the two PDFs, and the two potentials correspond to densities separated by a free-energy discontinuity, the transfer of ions between the 1st coordination shell and the 2nd shell (located at the Friedel oscillation minimum) has to be a cooperative process to produce such a discontinuity. This is done cooperatively and sharply because the densities are associated with the structures via the $2k_F$ scattering, linking the Fermi length ($1/k_F$) to the Wigner-Seitz length r_{ws}.

The coordination number in a liquid normally satisfies the limits

$$4 \leq N_c \leq 12.$$

When N_c reaches 12 we have a fully close packed structure corresponding to a solid. Hence, if the density were increased beyond 3.0 g/cm^3 towards 6.0 g/cm^3, one may envisage additional LPTs with the formation of a high-density form of silicon when N_c reach 12. However, these possibilities need further investigations. Similarly, one may expect that the LPT2 at 1200K is a precursor to a non-metallic LDL of the sort found in DFT-MD at LPT2.5.

D. Results for the PDFs and the structure factor

In this section we review some of our results from DFT-MD, NPA and compare them with experimental data where available.

E. PDFs

As the ion-ion correlations and the effect of transient bonding effects are of great interest to us, we compare in Fig. 5 the various calculated $g(r)$, with the experimental $g(r)$ extracted from X-ray scattering [39], for temperatures slightly above the melting point.

From Fig. 5 we see that the MD-DFT-SCAN and the NPA both recover the first peak with an under-estimate of the 1st experimental peak by about 5%. The first minimum near 3.05Å is not correctly reproduced by DFT-PBE (not shown) while DFT-SCAN and the NPA recover the first minimum position and height well. The second peak position (experiment at 1793 K 3.5 Å) and beyond are poorly recovered both by DFT-MD and by NPA. These observations may also be confirmed from

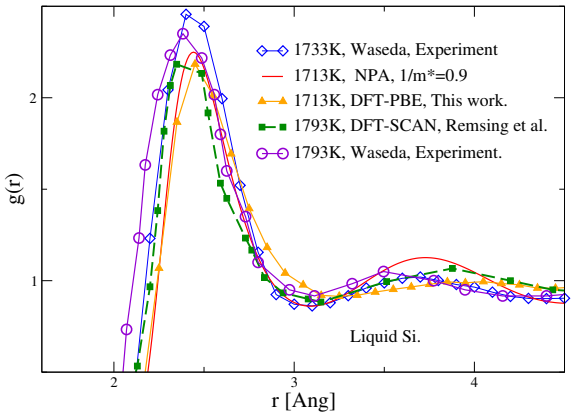

FIG. 5: (Online color) The ion-ion pair distribution $g(r)$ of Si at 1713K from MD-DFT and from NPA-HNC are shown here. The modification of the DOS at the Fermi energy are accounted for via an m^*. The experimental $g(r)$ reported by Waseda [39] is shown for comparison. The slight differences in temperature and density are negligible. It is seen that the first peak position and the first minimum are in good accord with the NPA, while the NPA over-estimates the second peak. The MD-simulation begins to differ from the first minimum and underestimates the peak heights.

Fig.1 of Remsing et al. [12] and also from Fig. 11 of their supplemental material. The NPA shows stronger secondary peaks compared to the experimental data, while the MD-DFT shows a weakly coupled liquid beyond the first neighbour.

F. Structure factor

The disagreement at the first peak of the S(k) between experiment and theory is more serious than for $g(r)$, as may be seen from Fig. 5 of the main text, from Fig. 11 of the supplemental material of Remsing et al [12], or from Fig. 2 of Ref. [24]. In the latter we have given the $S(k)$ from the NPA for both $m^* = 1.1$ and 1. The experimental data are from the 1980s, but no recent data seem to be available.

In Fig. 6 we display the variation of $S(k)$ as a function of the effective mass m^*. It shows how electron localization effects alter the ion-ion structure factor via $2k_F$ scattering. In effect, while detailed bonding descriptions are can be used and are in fact needed in the N-atom XC functionals, the one-atom DFT has to rely on the one-body self-energy and the electron-electron PDFs (via their local-field factors, Eq. 10) for treating all the complex structural features of these complex fluids.

While the main peak of $S(k)$ obtained from the NPA calculations for the case $m^* = 1$ recovers the height of the experimental $S(k)$, it does not recover the shoulder

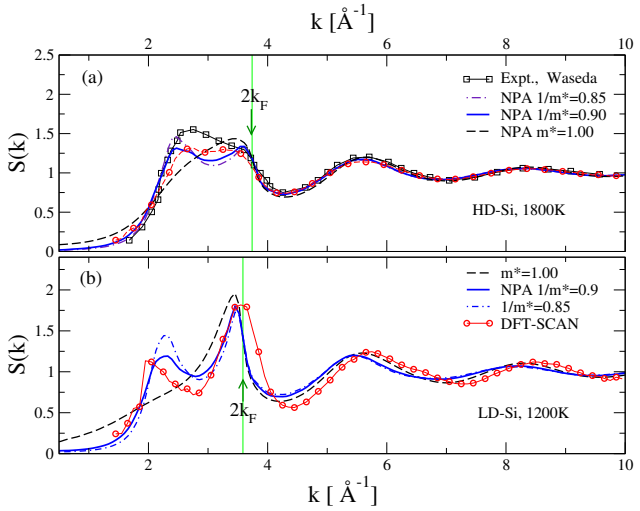

FIG. 6: (Online color) See Fig. 5. The dependence of the Si-Si structure factor on the effective-mass parameter m^*, and how the value of $S(k = 2k_F)$ is augmented at the cost of the main peak as mi^* changed, affecting $2k_F$ scattering. (a)Upper panel shows results for the high-density liquid. (b) The lower panel shows the even higher sensitivity of the low-density liquid on m^* and on $2k_F$ scattering.

found in the experimental data. While the usual chemical picture rationalizes these in terms of transient covalent bonding and the formation of different types of coordination states around the central ion, an equivalent but complementary picture is afforded by the gradation in the mean ionization $\bar{Z}$ between 4 and 3 being possible due to different mixtures and distributions of the two types of neutral pseudo atoms. This implies the existence of a mixture of Fermi liquids where the local band structure near k_F is associated with values of m^* in the range 1.0-1.2 of the electron mass. The $2k_F$ scattering contributes to the self-energy of the electrons and modifies the effective mass and the density of states near $2k_F$.

Figure 7, panel (a) displays the experimental data of Waseda [39] at 1733K. The experimental $S(k)$ near $2k_F$ is poorly recovered both by NPA-HNC and by MD-DFT. No experiments are available for the LDLs. Both $S(k)$ and $g(r)$ for HDL-Si from DFT-MD-SCAN agree with NPA results, exhibiting the split-structure of the first peak, while the higher-k sub peak falls at $\sim 2k_F$. The low-k subpeak at ~ 2 Å^{-1} registers with the low-k structure in the crystal $S(k)$, especially for the DFT-MD-SCAN result for LDL-Si at 1200K.

[1] P. F. McMillan, M. Wilson, D. Daisenberger and D. Machon Nat. Mater. 4, 680 (2005)
[2] Dominik Daisenberger, Mark Wilson, Paul F. McMillan, and Raul Quesada Cabrera, Martin C. Wilding, Denis Machon, Phys. Rev. B **75**, 224118 (2007)
[3] E. E. McBride, A. Krygier, A. Ehnes, E. Galtier, M. Harmand, Z. Konôpková, H. J. Lee, H.-P. Liermann, B. Nagler, A. Pelka, M. Rödel, A. Schropp, R. F. Smith, C. Spindloe, D. Swift, F. Tavella, S. Toleikis, T. Tschentscher, J. S. Wark and A. Higginbotham. Nature Phys. **15**, 89-94 (2019).
[4] A. Ng, T. Ao, F. Perrot, M.W.C. Dharma-wardana, M.E. Foord Laser and particle beams, **23**, 527-537 (2005)
[5] M. Baye *et al.* , Martin Beye, Florian Sorgenfrei, William F. Schlotter, Wilfried Wurth, and Alexander Föhlisch, PNAS, **28**, 16772 (2010)
[6] S. Sastry and C. A. Angell, Nat. Mater. **2**, 739 (2003)
[7] P. Beaucage and N. Mousseau, J. Phys. Condens. Matter **17**, 2269 (2005)
[8] V. V. Vasisht, S. Saw, and S. Sastry, Nat. Phys. **7**, 549 (2011)
[9] M. W. C. Dharma-wardana and F. Perrot, Phys. Rev. Lett., **65**, 76 (1990).
[10] T. Morishita, Phys. Rev. Lett. **93**, 055503 (2004).
[11] T. Morishita, Phys. Rev. Lett. **97**, 165502 (2006).
[12] Richard C. Remsing, Michael L. Klein and Jianwei Sun, Phys Rev B **97**, 140103(R) (2018)
[13] M. W. C. Dharma-wardana, Phys. Rev. B **100**, 155143 (2019)
[14] *VASP*- Vienna ab-initio simulation package: G. Kress, J. Furthmüller and J. Hafner, `http://cms.mpi.univie.ac.at/vasp/`; *ABINIT*, X.Gonze, B. Amadon, P.-M.Anglade, *et al.* Computer Physics Com. **180**,2582 (2009).
[15] F. Perrot and M. W. C. Dharma-wardana, Phys. Rev. B **62**, 16536 (2000); *Erratum:* **67**, 79901 (2003); arXive-1602.04734.
[16] M. W. C. Dharma-wardana and F. Perrot, Phys. Rev. A **26**, 2096 (1982)
[17] F. Perrot, Phys. Rev. E **47** 570 (1993).
[18] E. K. U. Gross, and R. M. Dreizler, *Density Functional Theory*, NATO ASI series, **337**, 625 Plenum Press, New York (1993).
[19] F. Perrot and M.W.C. Dharma-wardana, Phys. Rev. E. **52**, 5352 (1995)
[20] M. S. Murillo, J. Weisheit, S. B. Hansen, and M. W. C. Dharma-wardana, Phys. Rev. E **87**, 063113 (2013).
[21] P.A. Sterne S.B. Hansen, B.G. Wilson, W.A. Isaacs, High Energy Density Phys. **3**, 278 (2007)
[22] Advances in Atomic and Molecuar Physics, **21**, 306 (1985)
[23] W. Kohn, Phys. Rev. B **33**, 4331(R) (1986)
[24] M. W. C. Dharma-wardana, Phys. Rev. E **86**, 036407 (2012).
[25] M.W.C. Dharma-wardana and G.C. Aers, Phys. Rev. B **28**, 1701 (1983)
[26] N. H. March, Can. J. of Phys., **65**, 219-240, (1987).
[27] I. Štich, R. Car, and M. Parrinello, Phys. Rev. Lett. **63**, 2240 (1989)
[28] Richard C. Remsing and Michael L. Klein, J. Phys. Chem 2020 https://dx.doi.org/10.1021/acs.jpcb.0c01798
[29] Harbour, L. and Förster, G. D. and Dharma-wardana, M. W. C. and Lewis, Laurent J. Physical review E **97**,043210 (2018).
[30] M. W. C. Dharma-wardana, Cont. Plasma. Phys. **58**, Issue2-3, 128-142 (2018) International Con-

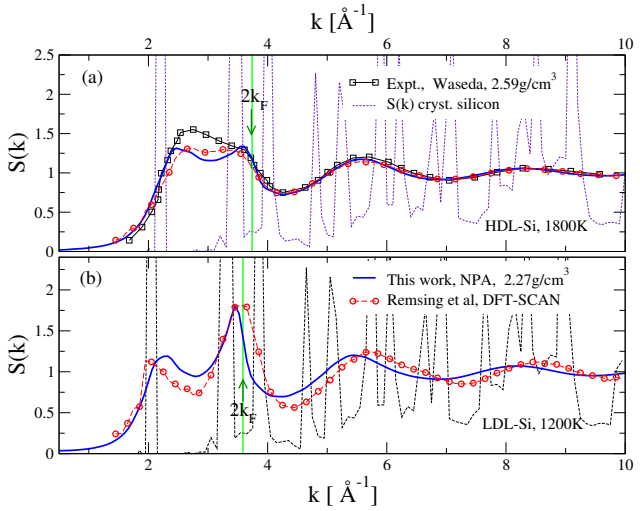

FIG. 7: (online color) (a) The $S(k)$ of HDL-Si at 1800K, 2.564 g/cm^3 from NPA is compared with the DFT-MD-SCAN [12]. The short dashed lines depict the $S(k)$ of *cry*-Si. Experimental data [39] for *l*-Si are at 1733K. (b) Theoretical $S(k)$ for the LDL-Si liquid at 1200k at the LPT. The major peak in the $S(k)$ of Ref. [12] is at $2k_F$, but broader.

ference Strongly Coupled Coulomb Systems July 30th- August 4th, 2017, Kiel, Germany, Part II https://doi.org/10.1002/ctpp.201700202

[31] L. Harbour, M. W. C. Dharma-wardana, D. Klug and L. Lewis, Physical Review E **94**, 053211, (2016).

[32] M. W. C. Dharma-wardana, Contrib. Plasma Phys. **55**, No.2-3, 79-81 (2015).

[33] V. Recoules, P. Renaudin, J. Clérouin, P. Noiret, and G. Zérah, Phys. Rev. E **66**, 056412 (2002).

[34] M.W.C. Dharma-wardana, D. D. Klug, L. Harbour, Laurent J. Lewis, Phys. Rev. E **96**, 053206 (2017).

[35] P. L. Rossiter, *The electrical resistivity of metals and alloys*, Cambridge University Press (1987).

[36] M Itoh and M Watabe J. Phys. F: Met. Phys. *14* L9 (1984)

[37] Monica Pozzo, Michael P. Desjarlais, and Dario Alfè, Phys. Rev. B, **84**, 054203 (2011).

[38] K. P. Migdal, V. V. Zhakhovsky, A. V. Yanilkin, Yu. V. Petrov, N. A. Inogamov Applied Surface Science, **478** 818 (2019).

[39] Yoshio Waseda, *Structure of Non-crystalline Materials*, McGraw-Hill, New York (1980
)